Diffraction, Radiation and Propagation of Elastic Waves in Isotropic and Anisotropic Bodies

Diffraction, Radiation and Propagation of Elastic Waves in Isotropic and Anisotropic Bodies

By

Alexander Kleshchev

Cambridge
Scholars
Publishing

Diffraction, Radiation and Propagation of Elastic Waves in Isotropic and Anisotropic Bodies

By Alexander Kleshchev

This book first published 2019

Cambridge Scholars Publishing

Lady Stephenson Library, Newcastle upon Tyne, NE6 2PA, UK

British Library Cataloguing in Publication Data
A catalogue record for this book is available from the British Library

ISBN (10): 1-5275-3993-8
ISBN (13): 978-1-5275-3993-8

The monograph presents the main results of the author's published research on the diffraction, radiation, and propagation of elastic waves.

1. *Hydroacoustic scatterers*. St. Petersburg: Sudostroenie, 1992 (1st ed.); Prima, 2012 (2nd ed.).
2. *The diffraction and propagation of waves on elastic media and bodies*. St. Petersburg: Vlas, 2002.
3. *The diffraction, radiation, and propagation of elastic waves*. St. Petersburg: Profprint, 2006.

In this book, the author's main ideas and results have been developed from his previous monographs.

CONTENTS

PREFACE

In recent years, there has been an increase in interest in problems in the field of the diffraction, radiation, and propagation of elastic waves that are associated with the interaction of bodies both with each other and with media interfaces. In addition, a great deal of attention has recently been paid to solutions to three-dimensional wave problems (with the help of Debye potentials) for elastic isotropic and anisotropic bodies of analytical and non-analytical forms.

The seventh chapter of this monograph provides the characteristics of the sound scattering (scattering cross-sections and angular diagram) of prolate and oblate spheroids, as well as theWatson transformation for ideal spheroids. The same chapter investigates an acoustic model of the agitated sea surface. In the eighth chapter, we will study the use of equations and diffraction theory methods for problems related to the synthesis of hydroacoustic antennas. In chapter nine, we will investigate the scattering of sound by elastic and viscoelastic bodies in the form of an infinite circular cylinder. The author has tried to consider all of these tendencies and trends when writing this monograph.

The research into the characteristics of sound scattering by spheroidal bodies was performed by S. A. Bespalova, E. Sedola, and A. P. Eglaya, under the direction of the Doctor of Physical and Mathematical Sciences, Yu. A. Klokov.

The calculations for the phase velocities in cylindrical bodies were carried out by S. L. Il'menkov and K. A. Klyubina. E. I. Kuznetsova performed the calculations for diffracted and radiated pulses. The author is also grateful V. Yu. Chizhov, G. K. Evstatiev, V. M. Kuz'kin, F. F. Legusha, and S. A. Peresyolkov for their helpful comments on the research results.

B. Ivanov and M. Moshchuk actively participated in the experiment to find the amplitude-phase characteristics of the scattering field of models in the Fresnel zone.

The author thanks V. I. Gromova, S. M. Kleshchev, A. S. Klimenkov, and M. M. Pavlov. I would also like to thank the CSP team, including Helen Edwards, Joanne Parsons, and Ivan Veller, for editing, proofreading, and publishing my manuscript.

CHAPTER 1

THE RESONANCES OF ELASTIC SPHEROIDAL BODIES

1.1. Solution to the Problem of the Diffraction of Sound from an Elastic Spheroidal Body using Debye's Potentials

In this section, the resonances of prolate and oblate spheroidal bodies (in their entirety and in the form of shells), which are impacted by three-dimensional and axisymmetric angles of irradiation, will be investigated. Debye's potentials have been used to calculate the three-dimensional pattern of irradiation in order to solve the diffraction problem. Various publications are devoted to the resonances of elastic spheroidal bodies [1–9].

Debye first proposed expanding the vector potential $\vec{A}$ and the scalar potentials U and V in his publication [10], which is devoted to studying the behavior of light waves near the local point or line. Later, this approach was used to solve the diffraction problems in the electromagnetic wave diffraction of a sphere, a circular disk, and a paraboloid revolution [11–16], as well as for the diffraction by spheroidal bodies in longitudinal and transverse waves [7, 17]. When Debye's potentials are applied to problems based on the theory of dynamic elasticity, it occurs as follows: the displacement vector $\vec{u}$ of an elastic isotropic medium obeys the Lame equation

$$(\lambda + \mu) graddiv\vec{u} - \mu curlcurl\vec{u} = -\rho\omega^2\vec{u}, \quad (1.1)$$

where λ and μ are Lame constants, ρ is the density of the isotropic medium, and ω is the circular frequency of harmonic vibrations. According to the Helmholtz theorem, the displacement vector $\vec{u}$ is expressed through scalar Φ and vector $\vec{\Psi}$ potentials as follows:

$$\vec{u} = -grad\Phi + curl\vec{\Psi} \quad (1.2)$$

Substituting E. (1.2) in E. (1.1), we obtain two Helmholtz equations, which include one scalar equation for Φ and one vector equation for $\vec{\Psi}$:

$$\Delta\Phi + h^2\Phi = 0, \quad (1.3)$$
$$\Delta\vec{\Psi} + k_2^2\vec{\Psi} = 0. \quad (1.4)$$

Here $h = \omega/c_1$ is the wavenumber of the longitudinal elastic wave; c_1 is the velocity of this wave; $k_2 = \omega/c_2$ is the wavenumber of the transverse elastic wave; and c_2 is the velocity of the transverse wave. In the three-dimensional case, the variables involved in scalar equation (1.3) can be separated into 11 coordinate systems. As for equation (1.4), in the three-dimensional problem, it yields three independent equations for each of components of the vector function $\vec{\Psi}$ in the Cartesian coordinate system alone. To overcome this difficulty, one can use Debye's potentials U and V, which obeys the Helmholtz scalar equation as follows:

$$\Delta V + k_2^2 V = 0; \Delta U + k_2^2 U = 0. \quad (1.5)$$

The vector potential $\vec{\Psi}$ (according to Debye) is expanded in potentials V and U as follows:

$$\vec{\Psi} = curlcurl(\vec{R}U) + ik_2 curl(\vec{R}V), \quad (1.6)$$

where $\vec{R}$ is the radius vector of a point of the elastic body or the elastic medium.

Let us demonstrate the efficiency of using Debye's potentials to solve the three-dimensional diffraction problems in the acoustical diffraction of an elastic spheroidal shell. The advantage of the representation (6) becomes evident, if we take into account that potentials V and U obey the Helmholtz scalar equation. It is convenient to represent components of $\vec{\Psi}$ in the spherical coordinate system by expressing them through U, V, and $\vec{R}$ and then, using vector analysis formulas, to change to spheroidal components. The expressions for spherical components of the vector function $\vec{\Psi}(\Psi_R, \Psi_\theta, \Psi_\varphi)$ in terms of Debye's potentials take the following form [7]:

$$\Psi_R = (\partial\xi/\partial R)^2(\partial^2 B/\partial\xi^2) + 2(\partial\xi/\partial R)(\partial\eta/\partial R)(\partial^2 B/\partial\xi\partial\eta) + (\partial\eta/\partial R)^2(\partial^2 B/\partial\eta^2) + (\partial^2\xi/\partial R^2)(\partial B/\partial\xi) + (\partial^2\eta/\partial R^2)(\partial B/\partial\eta) + k_2^2 B, \quad (1.7)$$

$$\Psi_\theta = [h_0(\xi^2 - 1 + \eta^2)]^{-1}[(\partial\xi/\partial\theta)(\partial\xi/\partial R)(\partial^2 B/\partial\xi^2) + (\partial\xi/\partial\theta)(\partial\eta/\partial R)(\partial^2 B/\partial\xi\partial\eta) + (\partial\xi/\partial R)(\partial\eta/\partial\theta)(\partial^2 B/\partial\xi\partial\eta) + (\partial\eta/\partial R)(\partial\eta/\partial\theta)(\partial^2 B/\partial\eta^2) + (\partial B/\partial\xi)(\partial^2\xi/\partial R\partial\theta) + (\partial B/\partial\eta)(\partial^2\eta/\partial R\partial\theta)] + ik_2(\sin\theta)^{-1}(\partial V/\partial\varphi), \quad (1.8)$$

$$\Psi_\varphi = [h_0(\xi^2 - 1 + \eta^2)^{1/2}\sin\theta]^{-1}[\partial\xi/\partial R)(\partial^2 B/\partial\xi\partial\varphi) + (\partial\eta/\partial R)(\partial^2 B/\partial\eta\partial\varphi) - ik_2 \times [(\partial\xi/\partial\theta)(\partial V/\partial\xi) + (\partial\eta/\partial\theta)(\partial V/\partial\eta)], \quad (1.9)$$

$$B = h_0(\xi^2 - 1 + \eta^2)^{1/2}U; -1 \le \eta \le +1; 1 \le \xi \le +\infty.$$

Spheroidal components of the function $\vec{\Psi}(\Psi_\xi, \Psi_\eta, \Psi_\varphi)$ are expressed as follows [7]:

$$\Psi_\xi = \Psi_R(h_0/h_\xi)\xi(\xi^2 - 1 + \eta^2)^{-1/2} + \Psi_\theta(h_0/h_\xi)(\xi^2 - 1 + \eta^2)^{1/2}(\partial\theta/\partial\xi), \quad (1.10)$$

$$\Psi_\eta = \Psi_R(h_0/h_\eta)\eta(\xi^2 - 1 + \eta^2)^{-1/2} + \Psi_\theta(h_0/h_\eta)(\xi^2 - 1 + \eta^2)^{1/2}(\partial\theta/\partial\eta), \quad (1.11)$$

$$\Psi_\varphi \equiv \Psi_\varphi, \quad (1.12)$$

$$h_\xi = h_0(\xi^2 - \eta^2)^{1/2}(\xi^2 - 1)^{1/2}; h_\eta = (\xi^2 - \eta^2)^{1/2}(1 - \eta^2)^{1/2}.$$

Let us consider a scatterer in the form of an isotropic elastic spheroidal shell (Fig. 1-1). All potentials, including the plane wave potential Φ_0, the scattered wave potential Φ_1, the scalar shell potential Φ_2, Debye's potentials U and V, and the potential Φ_3 of the gas filling the shell can be expanded in spheroidal functions:

$$\Phi_0 = 2\sum_{m=0}^{\infty}\sum_{n\ge m}^{\infty} i^{-n}\,\varepsilon_m \overline{S}_{m,n}(C_1,\eta_0)\overline{S}_{m,n}(C_1,\eta)R_{m,n}^{(1)}(C_1,\xi)\cos m\varphi, \quad (1.13)$$

$$\Phi_1 = 2\sum_{m=0}^{\infty}\sum_{n\ge m}^{\infty} B_{m,n}\overline{S}_{m,n}(C_1,\eta)R_{m,n}^{(3)}(C_1,\xi)\cos m\varphi; \quad (1.14)$$

$$\Phi_2 = 2\sum_{m=0}^{\infty}\sum_{n\ge m}^{\infty}[C_{m,n}R_{m,n}^{(1)}(C_l,\xi) + D_{m,n}R_{m,n}^{(2)}(C_l,\xi)]\overline{S}_{m,n}(C_l,\xi)\cos m\varphi; \quad (1.15)$$

$$\Phi_3 = 2\sum_{m=0}^{\infty}\sum_{n\ge m}^{\infty} E_{m,n}\,R_{m,n}^{(1)}(C_2,\xi)\overline{S}_{m,n}(C_2,\eta)\cos m\varphi; \quad (1.16)$$

$$U = 2\sum_{m=1}^{\infty}\sum_{n\ge m}^{\infty}[F_{m,n}R_{m,n}^{(1)}(C_t,\xi) + G_{m,n}R_{m,n}^{(2)}(C_t,\xi)]\overline{S}_{m,n}(C_t,\eta)\sin m\varphi; \quad (1.17)$$

$$V = 2\sum_{m=0}^{\infty}\sum_{n\ge m}^{\infty}[H_{m,n}\,R_{m,n}^{(1)}(C_t,\xi) + I_{m,n}R_{m,n}^{(2)}(C_t,\xi)]\overline{S}_{m,n}(C_t,\eta)\cos m\varphi, \quad (1.18)$$

$\bar{S}_{m,n}(C_1,\eta)$represents the angular spheroidal function; $R_{m,n}^{(1)}(C_1,\xi)$, $R_{m,n}^{(2)}(C_1,\xi)$, and $R_{m,n}^{(3)}(C_1,\xi)$ represents the radial spheroidal functions of the first, second, and third kinds $C_l = hh_0$; $C_t = k_2h_0$; $C_1 = kh_0, k$ is the wavenumber of the sound wave in the liquid; $C_2 = k_1h_0, k_1$ is the wavenumber of the sound wave in the gas filling the shell; h_0 represents the half-focal distance; $B_{m,n}, C_{m,n}, D_{m,n}, E_{m,n}, F_{m,n}, G_{m,n}, H_{m,n}$and $I_{m,n}$ are unknown expansion coefficients.

Expansion coefficients are determined from the physical boundary conditions present at two surfaces of the shell (ξ_0 and ξ_1; see Fig. 1-1) [7]:

(i) The continuity of the normal displacement component at both of the boundaries ξ_0 and ξ_1;

(ii) The normal stress on the outside boundary of the elastic shell is equal to the sound pressure in the liquid (ξ_0) and the normal stress on the inner boundary of the shell is equal to the sound pressure in the gas (ξ_1);

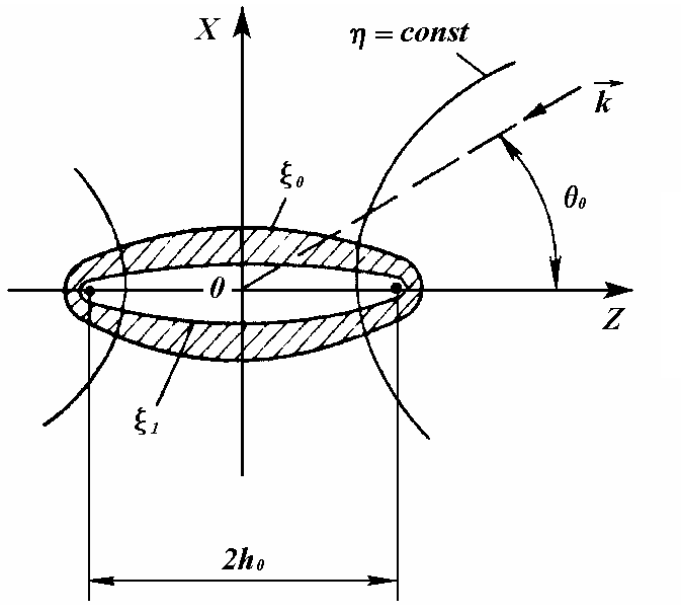

Figure 1-1: The elastic spheroidal shell in a harmonic plane wave field

(iii) The absence of tangential stresses at both of the shell boundaries, ξ_0 and ξ_1.

The corresponding expressions for boundary conditions take the following form [7]:

$$(h_\xi)^{-1}(\partial/\partial\xi)(\Phi_0+\Phi_1)=(h_\xi)^{-1}(\partial\Phi_2/\partial\xi)+(h_\eta h_\varphi)^{-1}[(\partial/\partial\eta)(h_\varphi\Psi_\varphi)-(\partial/\partial\varphi)(h_\eta\Psi_\eta)]_{\xi=\xi_0}; \quad (1.19)$$

$$(h_\xi)^{-1}(\partial\Phi_1/\partial\xi)=(h_\xi)^{-1}(\partial\Phi_2/\partial\xi)+(h_\eta h_\varphi)^{-1}[(\partial/\partial\eta)(h_\varphi\Psi_\varphi)-(\partial/\partial\varphi)(h_\eta\Psi_\eta)]_{\xi=\xi_1}; \quad (1.20)$$

$$-\lambda_0 k^2(\Phi_0+\Phi_1)=-\lambda h^2\Phi_2+2\mu[(h_\xi h_\eta)^{-1}(\partial h_\xi/\partial\eta)u_\eta+(h_\xi)^{-1}(\partial u_\xi/\partial\xi)]_{\xi=\xi_0}; \quad (1.21)$$

$$-\lambda_1 k_1^2\Phi_3=-\lambda h^2\Phi_2+2\mu[(h_\xi h_\eta)^{-1}(\partial h_\xi/\partial\eta)u_\eta+(h_\xi)^{-1}(\partial u_\xi/\partial\xi)]_{\xi=\xi_1}; \quad (1.22)$$

$$0=(h_\eta/h_\xi)(\partial/\partial\xi)(u_\eta/h_\eta)+(h_\xi/h_\eta)(\partial/\partial\eta)(u_\xi/h_\xi)_{\xi=\xi_0;\xi=\xi_1}; \quad (1.23)$$

$$0=(h_\varphi/h_\xi)(\partial/\partial\xi)(u_\varphi/h_\varphi)+(h_\xi/h_\varphi)(\partial/\partial\varphi)(u_\xi/h_\xi)_{\xi=\xi_0;\xi=\xi_1}, \quad (1.24)$$

where$h_\varphi=h_0(\xi^2-1)^{1/2}(1-\eta^2)^{1/2}$; $\lambda_0$is the bulk compression coefficient of the liquid and $\lambda_1$is the bulk compression coefficient of the gas filling the shell,

$$u_\xi=(h_\xi)^{-1}(\partial\Phi_2/\partial\xi)+(h_\eta h_\varphi)^{-1}[(\partial/\partial\eta)(h_\varphi\Psi_\varphi)-(\partial/\partial\varphi)(h_\eta\Psi_\eta)];$$
$$u_\eta=(h_\eta)^{-1}(\partial\Phi_2/\partial\eta)+(h_\xi h_\varphi)^{-1}[(\partial/\partial\varphi)(h_\xi\Psi_\xi)-(\partial/\partial\xi)(h_\varphi\Psi_\varphi)];u_\varphi=(h_\varphi)^{-1}(\partial\Phi_2/\partial\varphi)+$$
$$(h_\xi h_\eta)^{-1}[(\partial/\partial\xi)(h_\eta\Psi_\eta)-(\partial/\partial\eta)(h_\xi\Psi_\xi)].$$

The substitution of series (1.13)–(1.18) in boundary conditions (1.19)–(1.24) yields an infinite system of equations to determine the desired coefficients. Due to the orthogonality of the trigonometric functions, $\cos m\varphi$ and $\sin m\varphi$, the infinite system of equations breaks into infinite subsystems with fixed numbers, m. Each of the subsystems is solved using the truncation method. The number of retained terms of expansions (1.13)–(1.18) is increased with a greater wave size for the given potential.

The solution to the axisymmetric problem of sound waves diffraction from elastic spheroidal bodies has been presented in [1], [2], and [7–9].

1.2. Results of the Numerical Experiment to Determine the Low-Frequency Resonances from Elastic Spheroidal Bodies

The characteristics of the prolate gas-filled shell were calculated for two angles of irradiation: $\theta_0 = 0^0$ and $\theta_0 = 90^0$. In a different scale, Figure 1-2 presents the modules of the angular characteristics of the $|D(\theta)|$ scattering of a steel prolate gas-filled spheroidal shell (curve 1), a soft prolate spheroid (curve 2), and a hard spheroid (curve 3) impacted by the sound wave at an angle of $\theta_0 = 0^0$, where $C_1 = 1{,}0$.

Figures 1-3 and 1-4 present the same angular distributions, but (C_1 is the wave size) $C_1 = 3{,}1$ (for the elastic shell), $C_1 = 3{,}0$ (for the ideal spheroid), and $C_1 = 10{,}0$ (for the ideal spheroid). The notations of the curves for all three figures are identical. An analysis of the results shows that for an angle of $\theta_0 = 0^0$ and a wave dimension of $C_1 = 1{,}0$ (see Fig. 1-2), the angular characteristic of the elastic shell is similar to the characteristic of the hard spheroid. When $C_1 = 3{,}1$ and the irradiation angle of the impact is equal to $\theta_0 = 0^0$, the situation becomes indeterminate. The angular characteristic of the shell has a dipole character at the hard spheroid (see Fig. 1-3). In parallel with the increase of the wave dimension C_1, the character of the sound scattering from the shell remains complicated (see Fig. 1-4). In the lit region, the characteristic is $|D(\theta)|$ in the hard spheroid but, in the shaded region, it is nearer to the shade lobe of the soft spheroid than the shadow lobe of a hard spheroid. From known angular characteristics of $D(\theta, \varphi)$, the relative backscattering of the cross-sections (σ_0) from the elastic spheroidal bodies can be calculated [7]. Fig. 1-5 presents the mathematical term for the relative backscattering of cross-sections σ_0 of prolate spheroids with a semi axes correlation of 1:10 ($\xi_0 = 1{,}005$), which are impacted by the sound wave at an axially symmetric angle of irradiation ($\theta_0 = 0^0$). The behavior of the solid elastic spheroid is very similar to that of the ideal hard scatterer. This is seen through a comparison of the angular characteristics $D(\theta, \varphi)$ in steel and ideal spheroids. This is a coincidence and can be observed everywhere, with the exception of the resonance point, $C = 7{,}4$. This resonance is called a Rayleigh surface wave [5]. At a wave dimension of $C = 7{,}4$, the surface contour of the continuous steel prolate spheroid is $2{,}5\lambda_R$, where λ_R is the length of a Rayleigh-type wave. The velocity of the wave c_R is equal to 2889 m/s; however, on the planar boundary of the steel-vacuum, the velocity of the Rayleigh wave is equal to 2980 m/s.

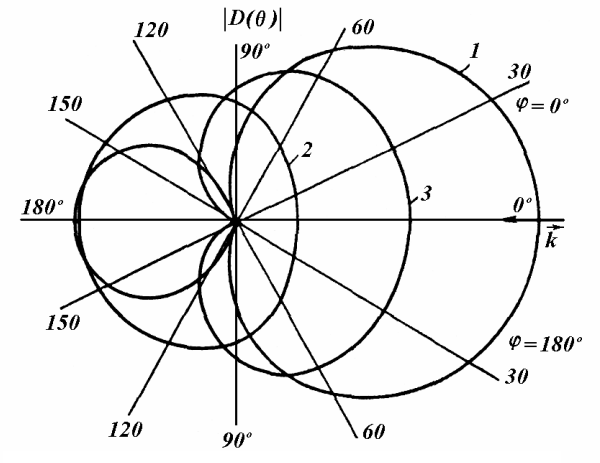

Figure 1-2: Modules of angular characteristics for spheroidal scatterers

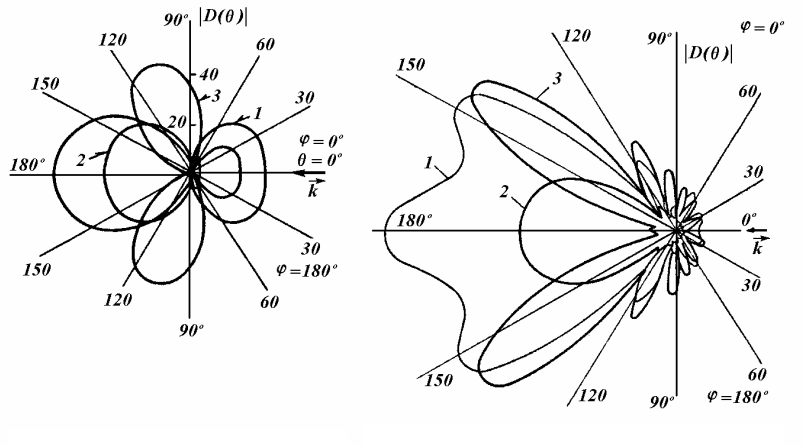

Figure 1-3 (left): Modules of the angular characteristics of spheroidal scatterers

Figure 1-4 (right): Modules of the angular characteristics of spheroidal scatterers

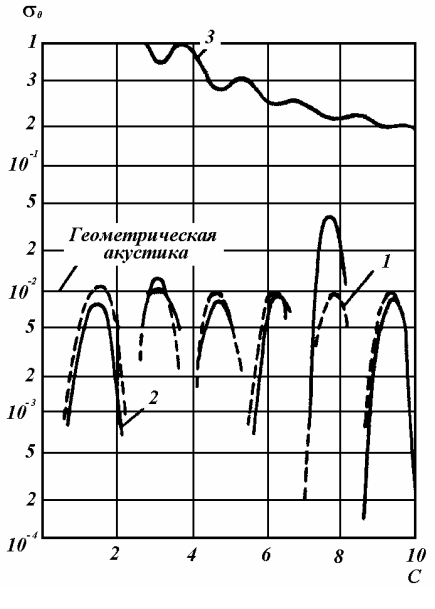

Figure 1-5: The relative backscattering of prolate spheroid cross-sections

Figure 1-6 presents the relative backscattering in the cross-sections σ_0 of oblate spheroids with a semi-axes correlation of 1:10 ($\xi_0 = 0{,}1005$) when, through an axially symmetric angle of irradiation $\theta_0 = 0^0$, the notations coincide with Figure 1-5. This will occur until the resonance of the zeroth antisymmetrical-flexural wave ($C \approx 5{,}3$) σ_0 of the steel oblate spheroid is closer to the σ_0 of the soft spheroid. Whereas for $C > 5{,}3$, it approaches the σ_0 of the hard spheroid, although the angular characteristic $D(\theta)$ obtained for the elastic spheroid at $\theta_0 = 0^0$ is for any wave size C close to the angular characteristic $D(\theta)$ of the hard spheroid.

Figure 1-7 presents sections σ_0 of prolate spheroidal scatterers. The steel prolate spheroid irradiated by the sound wave at an angle of $\theta_0 = 90^0$ has the resonance of the surface wave with the same meaning $C = 7{,}4$ (see curve 2, Fig. 1-5) [7]. The same section of the scattering σ_0 of the steel continuous spheroid (curve 3), which is irradiated by the sound wave at an angle of $\theta_0 = 90^0$, is visibly closer to the σ_0 of the hard spheroid (curve 4) in comparison with the σ_0 of the soft spheroid (curve 5). This similarity in the scattering properties of continuous elastic and hard spheroids was also shown in the angular characteristic $D(\theta, \varphi)$. The frequency dependence of the relative section σ_0 in the prolate spheroidal shell (curve 1) irradiated by the sound wave at an angle of $\theta_0 = 0^0$ shows the presence of considerable resonance by $C = 6{,}75$ [1, 7–9]. Figure 1-8 shows the modular uses of angular characteristics $|D(\theta)|$ in prolate spheroidal scatterers. Curve 1 is the steel, gas-filled shell with a wave dimension $C = 6{,}75$ that corresponds to its resonance. Curve 2 is a soft spheroid, while curve 3 is a hard spheroid. For all ideal spheroids, the wave size C is equal to 10,0.

From the comparison of the three curves, we can see that the shaded lobe of shell's angular characteristic is shown as the "soft background", but the lobe of the backscattering is shown as the "hard background".

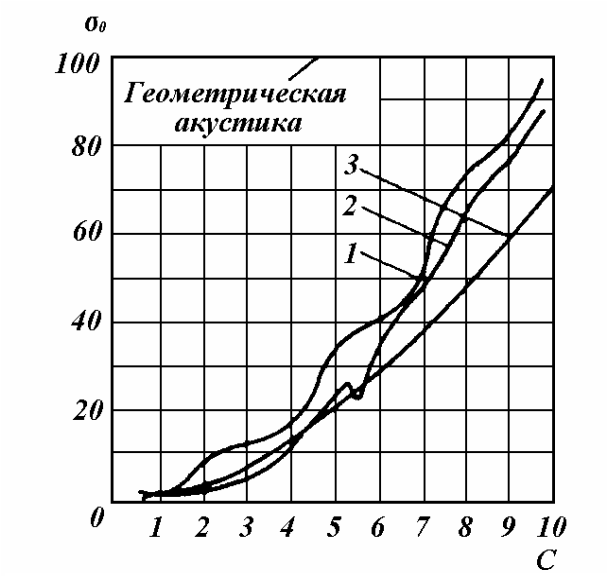

Figure 1-6: The relative backscattering in the cross-sections of oblate spheroids

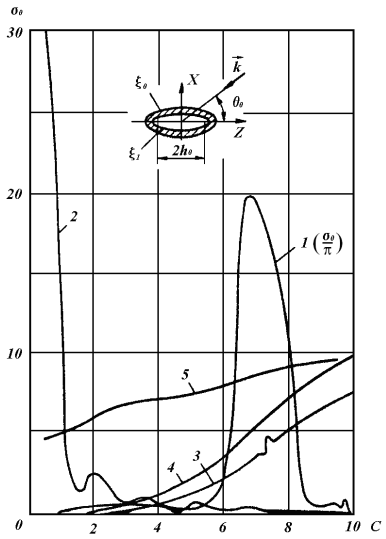

Figure 1-7: The relative backscattering in cross-sections of the prolate spheroidal scatterers

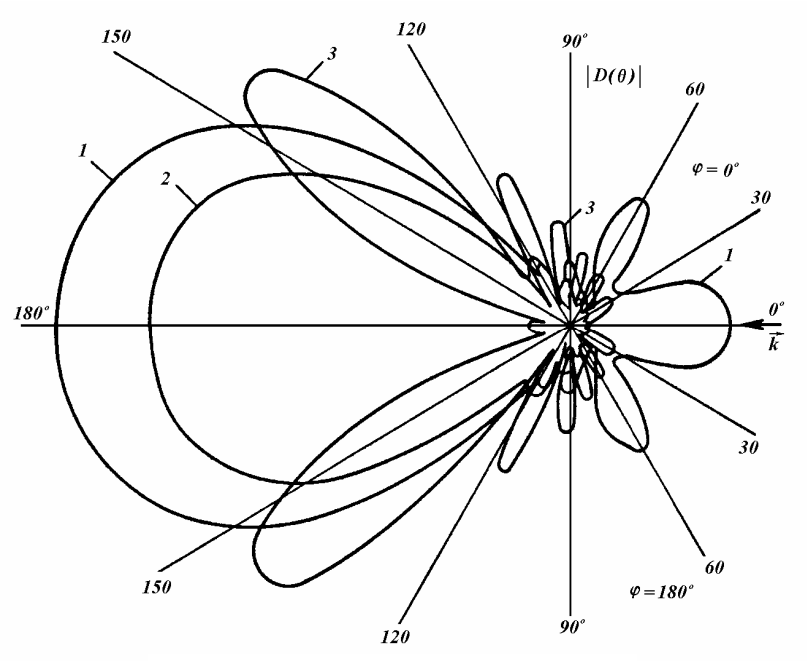

Figure 1-8: Modules with the angular characteristics of prolate spheroidal bodies

Table 1-1

Wave size C	σ_0 at an angle of $\theta_0 = 90°$		
	Spheroidal gas-filled shell $\xi_0 = 1{,}005075; \xi_1 = 1{,}005$	Hard spheroid $\xi_0 = 1{,}005$	Soft spheroid $\xi_0 = 1{,}005$
0,5	$0{,}3012 \cdot 10^{-3}$	$0{,}2452 \cdot 10^{-3}$	4,506
1,0	$0{,}4748 \cdot 10^{-2}$	$0{,}3908 \cdot 10^{-2}$	4,760
1,5	$0{,}2365 \cdot 10^{-1}$	$0{,}1965 \cdot 10^{-1}$	5,194
2,0	$0{,}7354 \cdot 10^{-1}$	$0{,}6147 \cdot 10^{-1}$	5,748
2,5	0,1751	0,1479	6,300
3,0	0,3470	0,3006	6,754
3,5	0,6068	0,5418	7,094
4,0	0,9736	0,8911	7,358
4,5	1,447	1,362	7,592
5,0	2,014	1,960	7,815
5,5	2,599	2,680	8,029

The relative backscattering of the cross-section σ_0 of a spheroidal shell irradiated by a sound wave at an angle of $\theta_0 = 90^0$ was calculated for a wave size ranging from C=0,5 to $C = 5{,}5$. The meanings of the σ_0 in a shell is very similar to the σ_0 in a hard spheroid; it is worthwhile to compare these sections in tabular form. As can be seen from Table 1-1, the angle of the shell's irradiation with wave sizes ranging from C=0,5 to $C = 5{,}5$ indicates a "hard background" to the scattering. This is what we can see from a comparison of the angular characteristics of the scattering $D(\theta, \varphi)$. A full scattering of the cross-section σ [7] is determined through the square of a modulus via the angular characteristic of the sound scattering $D(\theta, \varphi)$:

$$\sigma = \int_0^{\pi} \int_0^{2\pi} |D(\theta, \varphi)|^2 \, sin\, \theta \, d\theta d\varphi.$$

The relative scattering of the cross-section σ_r is equal to the following:

$$\sigma_r = \sigma / 2A_0,$$

where A_0 is depicted by the shaded geometrical region of the scatterer.

With the help of an optical theorem, a scattering cross-section σcan be found through the imaginary part of an angular characteristic in the direction of an incident wave (a forward scattering) $Im\, D\, (180^0 - \theta_0; 180^0)$ [7]:

$\sigma = (4\pi/k)\, Im\, D\, (180^0 - \theta_0; 180^0)$,

where θ_0 is the angle of the fall, $\varphi_0 = 0^0$.

Following the analogy with the scattering of a cross-section σ, it is possible to introduce the radiation cross-section σ_{rad} of an elastic or liquid body under the point source [7]:

$\sigma_{rad} = \int_0^{\pi} \int_0^{2\pi} |F(\theta, \varphi)|^2 \, sin\, \theta \, d\theta d\varphi$,

where $F(\theta, \varphi)$ is an angular characteristic of the sound radiation of a body subjected to the action of a point source.

On the basis of formulas presented, a full account was made of the total scattering cross-section σ and the relative cross-section σ_r. The radiation σ_{rad} should be moved off the cross-section σ_{rad} in the spheroidal prolate and oblate bodies. Figure 1-9 presents the sections of the scattering cross-section σ_r of an ideal hard oblate spheroid (curve 1), a steel oblate spheroid (curve 2), and an ideal soft oblate spheroid (curve 3). In all three cases, there is a relation between the semi-axes $a/b = 1{:}\, 10 (\xi_0 = 0{,}1005)$, but this has an irradiation angle of $\theta_0 = 0^0$. A relative section σ_r of an elastic spheroid shows the resonance of a coincidence, as in the case of the backscattering of σ_0 (see Fig. 1-6), but the maximum is displaced: for $\sigma_0$the maximum is observed at $C = 5{,}25$ but for σ_r it is $C - 5{,}35$. With an increase of C, curve 2 approaches $\sigma_r = 1{,}0$, thereby corresponding to the geometric acoustics calculations performed for an elastic oblate spheroid. This shows that at$C = 15{,}0$ section $\sigma_r = 0{,}866$, while at $C = 20{,}0 \rightarrow \sigma_r = 0{,}941$. Figure 1-10 presents the relative cross-sections of the scattering σ_r (curves 1 and 2) and the radiation σ_{rad} (curve 3) from prolate spheroidal bodies. Curve 1 shows the frequency dependence $\sigma_r(C)$ of an ideal soft prolate spheroid. Curve 2 corresponds $\sigma_r(C)$ to a steel gas-filled prolate spheroidal shell ($\xi_0 = 1{,}005075; \xi_1 = 1{,}005$). Both curves correspond to $\theta_0 = 0^0$ (an axially symmetric problem). Curve 2, for an elastic shell's relative backscattering section (curve 1 in Fig. 1-7) has two maximums (two resonances). The first maximum is observed at $C = 6{,}7$ (unlike from $C = 6{,}75$ for σ_0), while a second resonance is $C \approx 8{,}25$ and corresponds with $L = 1{,}5\Lambda$, where L is a length of a contour of the neutral surface of a shell, and Λ is the length of a longitudinal wave (a zeroth symmetrical Lamb's wave) that spreads with a velocity of $c_1 \approx 5420\ m/s$. Curve 1, for the ideal soft spheroid, asymptotically tends to the following geometric acoustical value:

$\sigma_r = 1{,}0)$: $\sigma_r(15{,}0) = 4{,}16; \sigma_r(65{,}0) = 2{,}23; \sigma_r(100) = 1{,}93.$

Curve 3 characterizes the radiating faculty of the same shell, if it is exited from the outside by a point source at an angle of $\theta_0 = 0^0 (h_0 = 50m)$. A section of the radiation σ_{rad} is at its most extreme point, and there is a relative section of σ_r. A comparison of curve 1 (in Fig. 1-7) with curves 2 and 3 (presented in Fig. 1-10) shows the relative backscattering cross-section when it does not provide sufficient information about resonant properties of elastic scatterers.

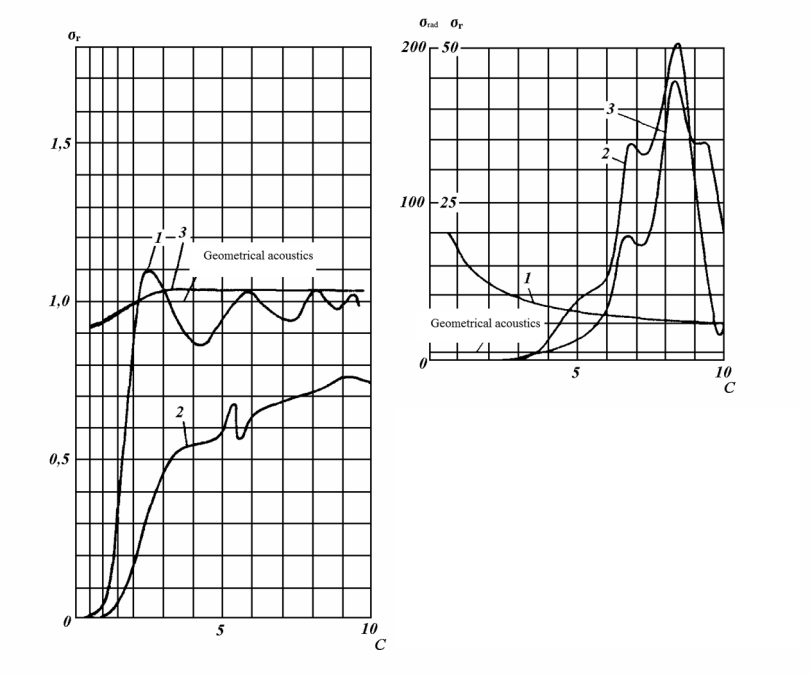

Figure 1-9 (left): The relative scattering of oblate spheroids cross-sections

Figure 1-10 (right): The relative scattering and radiating of prolate spheroidal bodies cross-sections

The results of the numerical calculations presented above make it possible to analyze the experimental amplitude-phase characteristics of the pulsed-sound signal scattering in the Fresnel and Fraunhofer zones [18, 19].

A series of recent publications [20–23] has demonstrated the efficiency of high-frequency asymptotes when calculating the diffraction fields of spheroids without using wave functions. It is remarkable that this approach is also valid for relatively low frequencies.

Resonances of elastic spheroidal shells (under axisymmetric excitation) have been studied in [24, 25]. In these publications, the authors considered steel and aluminum shells with different eccentricities and different thicknesses. For an aluminum shell with an axis ratio of 1:6 (an eccentricity of 0,995), the values of the normal velocity component were calculated. These revealed the presence of shell resonance at a wave size of C = 11,4 (recalculated according to the sound velocity in the liquid). In our steel shell with an axis ratio of 1:10 (an eccentricity 0,995), two resonances within the wave size interval 0,5–10,0 were observed for C=6,75 and C=8,25.

In [3], [5-6], [26–27], the resonances of elastic spheroidal shells were determined by the T-matrix method by applying the modified procedure to the extended Waterman method [26]. The function of the backscattering (scattering pattern) was calculated using the formulas proposed in [5]. Since the authors of these publications used spherical wavefunctions, the application of the T-matrices of dynamic elasticity theory in this method was limited to spheroidal axis ratios of 1:3. Our method of separating variables is free from this drawback.

CHAPTER 2

THE DIFFRACTION OF SOUND STATIONARY AND NON-STATIONARY IDEAL AND ELASTIC BODIES PLACED NEAR THE INTERFACE OF MEDIA IN AN UNDERWATER SOUND CHANNEL AND IN A PLANAR WAVEGUIDE

2.1. An Elastic Scatterer Near the Interface of Media

In the series of problems on the study of the influence of media interfaces on the characteristics of sound scattering by various bodies, the following variants are usually investigated:

a) The interaction of a scatterer with a single interface between media;
b) The scatterer in the field of interacting modes of the underwater sound channel; and
c) The finding of the total scattered field of the system of real and imaginary sources and scatterers of the planar waveguide.

The interaction of the scatterer with the interface between media is considered in the example of the scattering of sound by an elastic spheroidal body located at the interface between a liquid and an elastic medium [28]. Let the elastic gas-filled prolate spheroidal shell be placed near the boundary, a liquid, or an elastic medium (Fig. 2-1). The axis of rotation of the shell is parallel to the planar boundary. We introduced two systems of spheroidal coordinates ξ_s, η_s, φ_s ($s=1,2$): the first ($s=1$) is associated with the scatterer and the second ($s=2$) with the interface plane. The beginning of the Cartesian coordinate system O_2 and the foci of the second spheroidal coordinate system are defined as projections: O_1 and the foci of the first coordinate system on the plane of the boundary Z_2Y_2. The interfocus distance, $2h_0$, is common for both coordinate systems. The interface plane is two coordinate halves planes, $\phi_2' = \pi/2$ and $\phi_2'' = -\pi/2$, of the second coordinate system. In order to relate this solution to the solution of the problem of diffraction off of the elastic spheroidal shell, we simplify the formulation of the problem and assume that the wave vector $\vec{k}$ of the incident wave is in the X_1Z_1 plane and, correspondingly, in the X_2Z_2 plane as well: $\phi_{os} = 0°$ (see Fig. 2-1). Now, along with potential $\Phi_1^{(1)}$ of the wave and scattered by the shell, the potential $\Phi_1^{(2)}$ from the elastic half-space will appear as follows:

$$\Phi_1^{(2)} = 2\sum_{m=0}^{\infty}\sum_{n\geq m}^{\infty} K_{m,n}\bar{S}_{m,n}(C_1,\eta_2)R_{m,n}^{(1)}(C_1,\xi_2)\cos m\,\phi_2 \quad . (2.1)$$

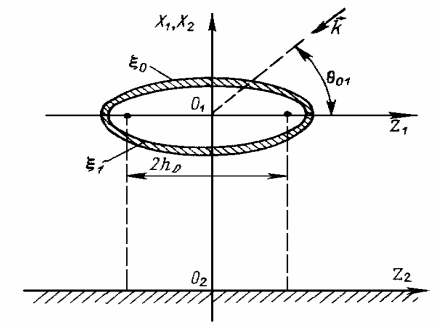

Figure 2-1: Elastic spheroidal shell near the liquid-elastic isotropic media interface

The potential $\Phi_1^{(2)}$ expands radial functions of the first kind. This is due to the fact that the foci of the second coordinate system lie in the plane of the interface. Physically, this means that the fields of pressure from two plane waves—an incident and when it is reflected by an interface—distort the scatters' interactions. Expansions in the shell's potentials are accompanied by expansions in the elastic half-space's potentials:

$$U_2^{(2)} = 2\sum_{m=1}^{\infty}\sum_{n\geq m}^{\infty} M_{m,n}\bar{S}_{m,n}(C_{t_2},\eta_2)R_{m,n}^{(1)}(C_{t_2},\xi_2)\sin m\,\phi_2 \quad ; (2.2)$$

$$W_2^{(2)} = 2\sum_{m=0}^{\infty}\sum_{n\geq m}^{\infty} N_{m,n}\bar{S}_{m,n}(C_{t_2},\eta_2)R_{m,n}^{(1)}(C_{t_2},\xi_2)\cos m\,\phi_2 \ ; (2.3)$$

$$\Phi_2^{(2)} = 2\sum_{m=0}^{\infty}\sum_{n\geq m}^{\infty} L_{m,n}\bar{S}_{m,n}(C_{l_2},\eta_2)R_{m,n}^{(1)}(C_{l_2},\xi_2)\cos m\,\phi_2 \ , (2.4)$$

where C_{l_2} and C_{t_2} are wave dimensions of longitudinal and transverse waves, respectively.

The potential of the incident wave Φ_0 in two coordinate systems has the following form [29, 30]:

$$\Phi_0 = 2\sum_{m=0}^{\infty}\sum_{n\geq m}^{\infty} i^{-n}\varepsilon_m\bar{S}_{m,n}(C_1,\eta_0)\bar{S}_{m,n}(C_1,\eta_s)R_{m,n}^{(1)}(C_1,\xi_s)\cos m\,\phi_s \ , (s=1,2) \ . (2.5)$$

The potential of a diffracted field $\Phi_\Sigma = \Phi_0 + \Phi_1^{(1)} + \Phi_2^{(2)}$ simultaneously meets the boundary conditions on both the surface of a shell and the planar interface between a liquid and an elastic medium. The boundary conditions on a surface of a shell are supplemented by the conditions of an interface on a liquid elastic medium:

$$\lambda_0 k^2\left(\Phi_0 + \Phi_1^{(1)} + \Phi_1^{(2)}\right) = \lambda_2 k_{l_2}^2\Phi_2^{(2)} + 2\mu_2 u_{\phi\phi}^{(2)}\Big|_{\phi=\pi/2;-\pi/2} \ ; (2.6)$$

$$\left(h_\phi^{(2)}/h_\xi^{(2)}\right)(\partial/\partial\xi)\left(u_\phi^{(2)}/h_\phi^{(2)}\right) + \left(h_\xi^{(2)}/h_\phi^{(2)}\right)(\partial/\partial\phi)\left(u_\xi^{(2)}/h_\xi^{(2)}\right)\Big|_{\phi=\pi/2;-\pi/2} = 0 \ ; (2.7)$$

$$\left(h_\phi^{(2)}/h_\xi^{(2)}\right)(\partial/\partial\xi)\left(u_\phi^{(2)}/h_\phi^{(2)}\right) + \left(h_\xi^{(2)}/h_\phi^{(2)}\right)(\partial/\partial\phi)\left(u_\xi^{(2)}/h_\xi^{(2)}\right)\Big|_{\phi=\pi/2;-\pi/2} = 0 \ ; (2.8)$$

$$-\left(h_\phi\right)^{-1}(\partial/\partial\phi)\left(\Phi_0 + \Phi_1^{(1)} + \Phi_1^{(2)}\right) =$$
$$= \left(h_\phi^{(2)}\right)^{-1}(\partial\Phi_2/\partial\phi) + \left(h_\xi^{(2)}h_\eta^{(2)}\right)^{-1}\left[(\partial/\partial\xi)\left(h_\eta^{(2)}\psi_\eta^{(2)}\right) - (\partial/\partial\eta)\left(h_\xi^{(2)}\psi_\xi^{(2)}\right)\right]\Big|_{\phi=\pi/2;-\pi/2} \ , (2.9)$$

where λ_2 and μ_2 represent Lame coefficients of an elastic half-space and $k_l^{(2)}$ represents the wave number of the longitudinal wave an elastic half-space.

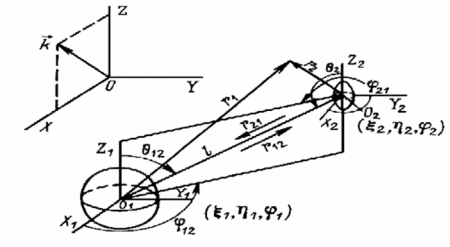

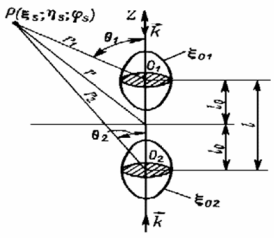

Figure 2-2 (left): Systems of spheroidal coordinates

Figure 2-3 (right): An ideal spheroid at associated with two interacting scatterers and a media interface

In our formulation, the evenness of the solution, with respect to the *XZ* planar boundary conditions for $\phi = -\pi/2$, completely repels the conditions for $\phi = +\pi/2$. Additionally, given the similarity between $\phi = -\pi/2$ and $\phi = +\pi/2$, there is no need to repeat the same kind of calculation for the other half of the scatterer, which is located on other side of the axis of symmetry, because doing so does not provide any additional information. When substituting potential expansions into boundary conditions for a shell and a planar interface when expansion coefficients are used an additional theorem for wave spheroidal functions [30] is as follows:

$$R_{p,q}^{(1),(3)}(C_j,\xi_j)\bar{S}_{p,q}(C_j,\eta_j)\,exp(ip\phi_j) = \sum_{n=0}^{\infty}\sum_{m=-n}^{n} R_{m,n}^{(1)}(C_s,\xi_s)\times$$
$$\times\,\bar{Q}_{m,n,p,q}^{(1),(3)}(C_j,C_s;l;\theta_{js})\bar{S}_{m,n}(C_s,\eta_s)\,exp(ip\phi_s) \ , (2.10)$$

where $\overline{Q}^{(l),(3)}_{m,n,p,q} = 2(-i)^{n-q}\sum_{r=0,1}^{\infty}{}'\sum_{t=0,1}^{\infty}{}' d_r^{pq}(C_j)d_t^{mn}(C_s)\sum_{\sigma=|r+p-t-m|}^{r+p+t+m}(-i)^{\sigma}\times$
$\times\tilde{b}_{\sigma}^{(r+p,p,t+m,m)}Z_{\sigma}^{(l),(3)}(kl)\tilde{P}_{\sigma}^{p-m}(\theta_{js})exp[i(p-m)\varphi_{js}];$

θ_{js} represents the polar angle of a point O_s which is the beginning of an *s*-th coordinate system in an *i*-th system (Fig. 2-2); l represents the distance between O_j and O_s; $d_r^{pq}(C_j)$ and $d_t^{mn}(C_s)$ represent the coefficients of the expansion of functions $\bar{S}_{p,q}(C_j,\eta_j)$ and $\bar{S}_{m,n}(C_s,\eta_s)$ by $\tilde{P}_r^p(\eta_j)$ and $\tilde{P}_t^m(\eta_s)$, which (up to a constant factor) coincide with normalized joined Legendre functions; $Z_{\sigma}^{(1)} = j_{\sigma}(kl)$ represents spherical Bessel functions; $Z_{\sigma}^{(3)} = h_{\sigma}^{(1)}(kl)$ represents spherical Hankel functions of the first kind coefficients $\tilde{b}_{\sigma}^{(r+p,p,t+m,m)}$ are obtained from coefficients $b_{\sigma}^{(r+p,p,t+m,m)}$ [30], taking into account a relationship $\tilde{P}_t^m(\eta_s)$and associated Legendre functions; a prime for signs Σ means that a summation of *r* and *t* is carried out on an even mean basis if, corresponding, *g* - *p* and *n* - *m* is even and a summation of *r* and *t* is carried of on an odd basis if *g* - *p* and *n* - *m* is odd.

A strict solution can be obtained for another orientation of a spheroidal shell with respect to the planar boundary—namely, due to the perpendicularity of the rotational axis of a shell in relation to the planar interface between liquid and elastic media (Fig. 2-3). We will consider this orientation in more detail by replacing a spheroidal shell with an ideal prolate soft spheroid and by replacing the elastic half-space with an ideal medium (hard or soft) [31]. We will map a scatterer and a source mirror-wise with respect to a boundary and so reduce the problem to one the diffraction of the fields of two sources (both real and imaginary) by two spheroidal scatterers (both real and imaginary). Potentials Φ_s (*S=1,2*) of waves scattered by spheroids are chosen in the form of expansions (taking axial symmetry into account) [31]:

$$\Phi_s(\xi_s,\eta_s) = \sum_{n=0}^{\infty} B_{0,n}^s \bar{S}_{0,n}(C_s,\eta_s)R_{0,n}^{(3)}(C_s,\xi_s)\ . (2.11)$$

Since spheroids (both real and imaginary ones) are ideally soft then, for their surfaces ($\xi_0=\xi_{01}=\xi_{02}$), the key requirement of a homogeneous Dirichlet is satisfied:

$$\Phi_0 + \sum_{s=1}^{2}\Phi_s = 0|_{\xi=\xi_0;s=1,2}\ . (2.12)$$

The potential of a falling plane wave is given by the following expansion:

$$\Phi_0(\xi_s,\eta_s) = 2\sum_{n=0}^{\infty} i^{-n}\bar{S}_{0,n}(C_s,\eta_s)R_{0,n}^{(1)}(C_s,\xi_s)\bar{S}_{0,n}(C_s,1) \quad s=1,2\ . (2.13)$$

Unknown coefficients $B_{0,n}^s$of expansions (2.11) are sought from an infinite system of equations and boundary conditions (2.12) [31]:

$$B_{0,n}^s + \sum_{q=0}^{\infty} B_{0,q}^t R_{0,n}^{(1)}(C_s,\xi_{0s})\left[R_{0,n}^{(3)}(C_s,\xi_{0s})\right]^{-1}\bar{Q}_{0n0q}^{(3)}(C_t,C_s;l;\theta_{ts}) =$$
$$= -2i^{-n}\bar{S}_{0n}(C_s,1)R_{0,n}^{(1)}(C_s,\xi_{0s})\left[R_{0,n}^{(3)}(C_s,\xi_{0s})\right]^{-1}, \quad s=1,2\ ; \quad t=1,2\ ; \quad s\neq t\ , (2.14)$$

where l represents the distance between centers of coordinate systems O_1 and O_2 (Fig. 2-3), in the given case

$$\theta_{12} = 0\ \theta_{21} = \pi$$

$$\bar{Q}_{0n0q}^{(3)}(C_t,C_s;l;\theta_{ts}) = 2i^{-n+q}\sum_{r=0,1}^{\infty}{}'\sum_{j=0,1}^{\infty}{}' d_r^{0q}(C_t)d_j^{0n}(C_s)\sum_{\sigma=|r-j|}^{r+j} i^{-\sigma}b_{\sigma}^{(r,0,j,0)}h_0^{(1)}(kl)P_{\sigma}(cos\,\theta_{ts})\ ;$$

$$.b_{\sigma}^{(r,0,j,0)} = (rj00|\sigma O)^2.$$

For the regularization of a system (2.14) with respect to unknown coefficients $B_{0,n}^s$ we introduce a new unknown $X_{0,n}^s$ [31]:

$$B_{0,n}^s = R_{0,n}^{(1)}(C_s,\xi_{0s})X_{0,n}^s\ . (2.15)$$

As a result, an infinite system (2.14) for unknown $B_{0,n}^s$is reduced to another infinite system of a relatively new unknown $X_{0,n}^s$ [31]:

$$X_{0,n}^{s} + \sum_{q=0}^{\infty} X_{0,q}^{t} R_{0,q}^{(1)}(C_t, \xi_{0t}) \left[R_{0,n}^{(3)}(C_s, \xi_{0s})\right]^{-1} \bar{Q}_{0n0q}^{(3)}(C_t, C_s; l; \theta_{ts}) =$$
$$= -2i^{-n} \bar{S}_{0,n}(C_s, 1) \left[R_{0,n}^{(3)}(C_s, \xi_{0s})\right]^{-1} . \quad (2.16)$$

Furthermore, by means of a truncation method, we find the solution of a regular system (2.16). Initially, we calculated the angular scattering functions $D_s(\theta_s)$ of two interacting spheroids, which distorted the monochromatic plane wave field. Fig. 2-4 shows the modules of angular characteristics $|D_s(\theta_s)|$ in interacting spheroids (curve 1 refers to the first spheroid, and curve 2 refers to the second spheroid). Curve 3 depicts another scale, $|D(\theta)|$, for a single soft spheroid in an infinite medium. The scale had to be changed so that curve 3 did not merge with curves 1 and 2. Curve 4 is characterized by the modulus $|D_\Sigma(\theta_1)|$ of a total angular characteristic in coordinates of a first spheroid (Fig. 2-1):

$$|D_\Sigma(\theta_1)| = |D_1(\theta_1) + D_2(\theta_1)\, exp(ikl\cos\theta_1)| .$$

Calculations were carried out for $C_1=C_2=10{,}0$, $\xi_{01}=\xi_{02}=\xi_0=1{,}005$, with a half-focus distance of $h_{01}=h_{02}=1$м, $l=8h_0$. An analysis of the curves presented in Fig. 2-4 shows that when selected parameters were (C_1, C_2, l), the interaction of scatterers turned out to be small and, because of this, the curves 1, 2, 3 are close to each other. The main role is played by the interference effects (especially in the shadow region); therefore, curve 4 stands out sharply (again in the shadow region) against the background of the other curves. In a second stage (based on a calculation of the scattered field of two spheroids), the angular characteristics $D_\Sigma(\theta)$ of a soft spheroid ($\xi_0=1{,}005$; $C=10$) located at a distance ($l_0=4h_0=4$ m) from an interface between the liquid and an ideal medium, were calculated. The results of the calculations $|D_\Sigma(\theta)|$ are shown in Fig. 2-5. Curve 1 corresponds to the interface between liquid and soft media.

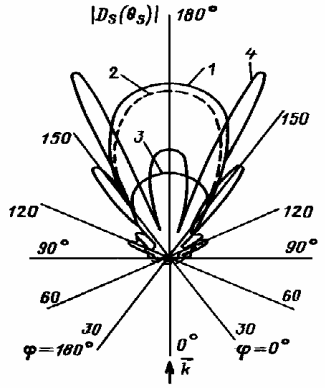

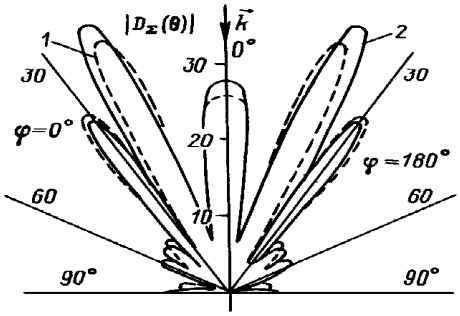

Figure 2-4 (left): Modules of the angular characteristics of single and interacting spheroids

Figure 2-5 (right): Modules of angular characteristics of a soft spheroid placed at the interface media

A certain contribution to $D_\Sigma(\theta)$ is made by an imaginary source and interference is associated with it along the fringes of both spheroids, including physically intense scattering in an illuminated region. This arises due to the reflection of the waves scattered by spheroids in the planar interface between media. We must not forget that, in this case, we are not talking about the distortion of a plane-traveling wave (as if it were an boundless medium) but we are, instead, talking about the distortion of a standing wave field that makes real and imaginary sources.

There is only one strict solution to the problem of the scattering of sound by a spheroidal half-body placed on the interface between a liquid and an ideal medium. Using the mirror image of a scatterer and a source connected to the planar boundary, we receive a spheroidal scatterer located in a field two sources (real and imaginary). A phase of a wave potential, from an imaginary source on a planar interface, coincides with a phase of a potential of an incident wave in a liquid, which borders on an ideally rigid medium. The phases of these waves differ from this boundary by 180˚ if the liquid borders on an ideally soft medium. Fig. 2-6 shows the modules of the angular characteristics $|D(\theta)|$ (in different scales) of spheroidal half-bodies located on the boundary between a liquid and an ideal medium. Curve 1 corresponds to half of a hollow steel oblate spheroidal shell placed on the boundary between a liquid and an ideally soft media. The outer radial coordinate of a shell is $\xi_0=0{,}1005$ and the internal is – $\xi_1=0{,}07669$. It has a wave size of $C=7{,}1$, and an irradiation angle of $\theta_0=0$˚(an axisymmetric problem). Two other curves (see Figure 2-6) relate to the modulus

of angular characteristics of a soft oblate hemispheroid bordering on a soft media (curve 2) and a hard media (curve 3) at the same angle of irradiation $\theta_0=0^\circ$ and the wave size of a body of $C=10,0$, with a radial coordinate of a soft oblate spheroid $\xi_0=0,1005$.

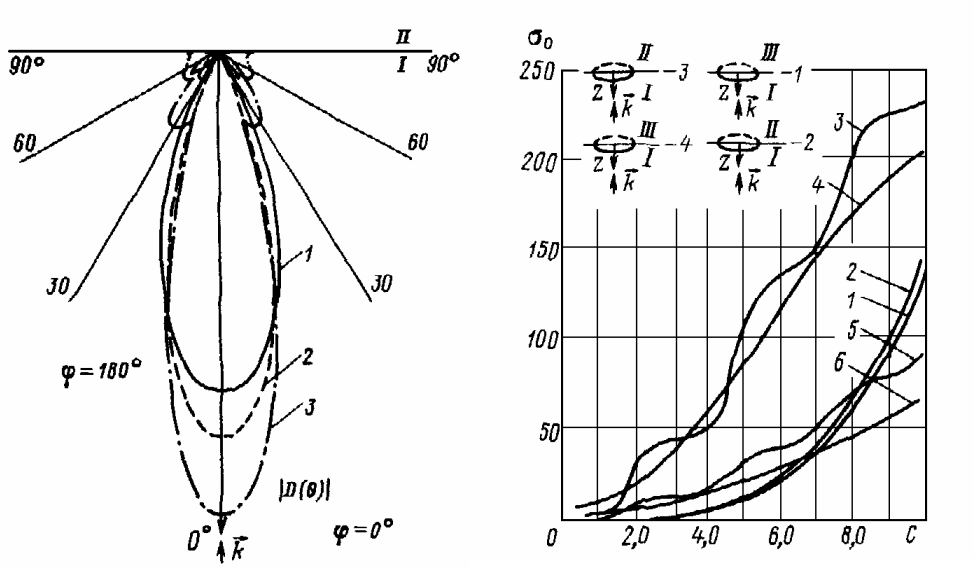

Figure 2-6 (left): Modules of angular characteristics of spheroidal semi-bodies located at an interface between the media

Figure 2-7 (right): Relative cross sections for the backscattering of oblate spheroids

Fig. 2-7 shows the relative cross-sections for the backscattering σ_0 of oblate ideal hemispheroids located at the interface between the two media, where by $D(\theta;\phi)$ we mean the total angular characteristics (from real and imaginary sources). Curves in Fig. 2-7 correspond to the axial radiation ($\theta_0=0^\circ$) of an oblate hemispheroid (soft or hard) with a radial coordinate of $\xi_0=0,1005$. Curves 1 and 3 refer to a hard hemispheroid placed at a boundary with (1) a hard media and (3) a soft media (we have designated the liquid as number "I", the soft media as number "II", and the hard media as number "III"). Curves 3 and 4 correspond to a soft hemispheroid located at a boundary between soft media ("2") and hard media ("4"). Curves 5 and 6 give an idea of the variation σ_0 between hard ("5") and soft ("6") oblate spheroids ($\xi_0=0,1005$) in an infinite liquid medium. It is easy to see that if a hemispheroid and an ideal semi-bounded medium (whether hard or soft; see curves 1 and 2) or a hemispheroid represents a distortion in the shape of a boundary, which hides this unevenness. If σ_0 grows slowly at small wave dimensions close to zero, then the hemispheroid and semi-bounded ideal medium cross-sections σ_0 will have much larger curves 3 and 4) across an entire investigated range of wave dimensions. While curves 5 and 6 tend asymptotically towards a value geometric acoustics, the remaining curves increase indefinitely. The mathematical and physical explanations for this phenomenon are given in the comments related to Fig. 2-5.

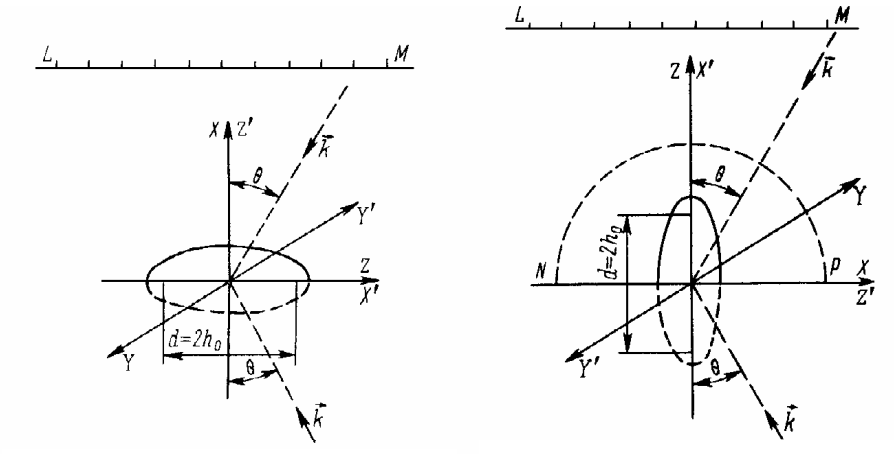

Figure 2-8 (left): The mutual orientation of a combined system and a hemispheroid (1st variant)

Figure 2-9 (right): The mutual orientation of a combined system and a hemispheroid (2nd variant)

Let us now turn to passive characteristics in a scattering indicatrix from hemispheroids located on an interface between a liquid and an ideal medium. We imagine that, for a fairly large distance from a boundary across, there is a combined system (source-receiver) which moves along a line *LM*. However, we are interested in a reflected signal to the point of the disposition in the combined system. The movement of the system is so slow that a Doppler effect can be ignored. Two admittedly possible orientations for the two half-bodies are depicted in Figs. 2-8 and 2-9. Fig. 2-10 presents (in different scales) modules $\left|D_{\Sigma}^{0}(\theta)\right|$for a prolate soft hemispheroid on the boundary of a liquid with an ideal hard medium (as depicted by curve 1, where the scale is to the left of the vertical axis, $\xi_0=1{,}005$, $C=10$) and for an oblate hard hemispheroid on the boundary of a liquid with an ideal l soft medium (as depicted by curve 2, the scale is to the right of the vertical axis, $\xi_0=0{,}1005$; $C=10$). A layout orientation of the two hemi-bodies corresponds to Fig. 2-8, and the directions of the rays meet the oblate coordinate system. Fig. 2-11 shows modules $\left|D_{\Sigma}^{0}(\theta)\right|$for a prolate hard hemispheroid at the boundary of a liquid with an ideally soft medium (a curve 1, $\xi_0=1{,}005$, $C=10$) and for an oblate hard hemispheroid on the boundary of a liquid with an ideally soft medium (a curve 2, $\xi_0=0{,}1005$; $C=10$). The orientation of the hemi-bodies corresponds to Fig. 2-9, and the directions of the rays meet the prolate coordinate system. The analysis presents a scattering indicatrix and shows the advantages of a second-type orientation (see Fig. 2-9; this is because it appears that an intense non-mirror component is associated with the sound reflective nature of the interface. With regard to an orientation of the first type (see Fig. 2-8), an intensive back-reflection at $\theta=0^{o}$ will be masked by the reflection from the planar interface.

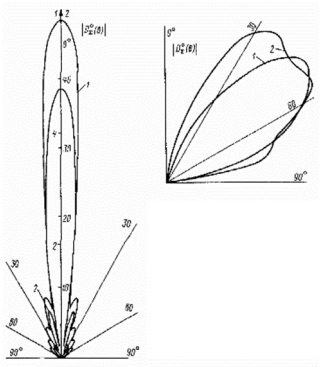

Figure 2-10 (left): Modules of scattering indicatrics of soft hemispheroids

Figure 2-11 (right): Modules of scattering indicatrics of hard hemispheroids

We will now move from examining stationary (harmonic) irradiation to non-stationary radiation in the form of sound pulses with a rectangular envelope and monochromatic filling. As before, we will consider media interfaces of three types: the boundary between a liquid and an elastic bottom; the boundary between a liquid and an ideally soft medium (the Dirichlet condition); and the boundary between a liquid and an ideally hard medium (the Neumann condition).

If a scatterer (an oblate hard spheroid) is placed at the interface between media (the boundary between a liquid and an elastic bottom) at an observation point, it will first accept the pulse of a mirror reflection from a scatterer.

Fig. 2-12a shows a mirror reflection pulse $r_1 \cdot \Psi_S(t)$ for a hard oblate spheroid when it is irradiated at an angle of $\theta_1 = 30°$; a normalized modulus of the spectrum of a pulse $r_1 \cdot \Psi_S(t)$ can be seen in Fig. 2-12b. After a while, the pulse $\Psi_{\Sigma}(t')$ will reach observation point *P*, which is reflected from an elastic bottom and diffracted on a spheroid.

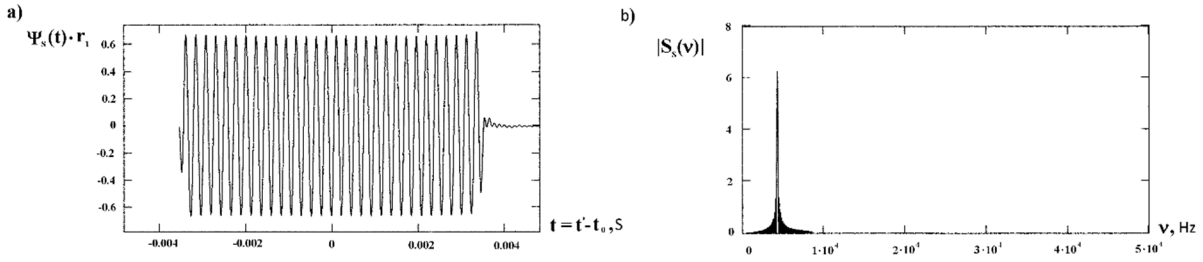

Figure 2-12a (left): A mirror reflection pulse $r_1 \cdot \Psi_S(t)$

Figure 2-12b (right): The normalized modulus of the spectrum $|S_S(\nu)|$ of a pulse $r_1 \cdot \Psi_S(t')$

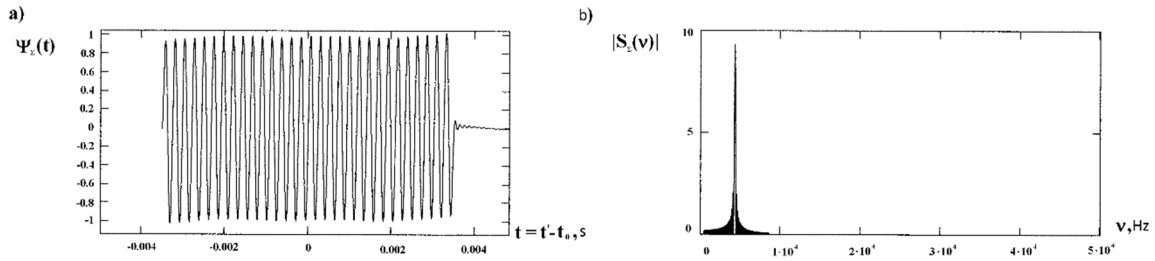

Fig. 2-13a (left) shows a pulse $\Psi_\Sigma(t)$. The normalized modulus spectrum $|S_\Sigma(\nu)|$ of a pulse $\Psi_\Sigma(t')$ is presented in Fig. 2-13b.

Figure 2-13b (right): The normalized modulus of the spectrum $|S_\Sigma(\nu)|$ of a pulse$\Psi_\Sigma(t')$

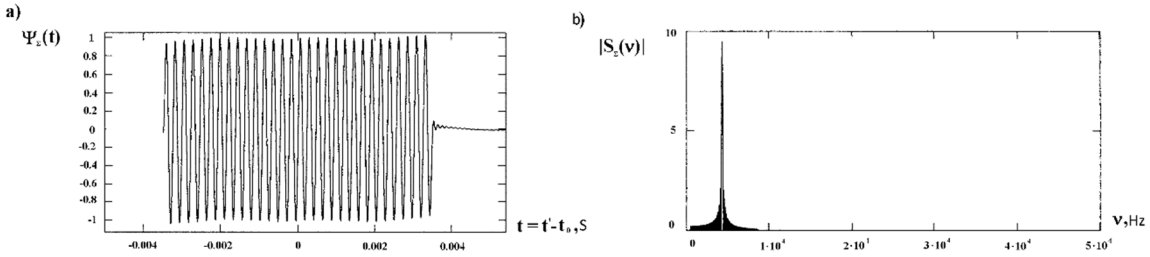

Figure 2-14a (left): A mirror image of the reflection pulse $\Psi_\Sigma(t)$ for a hard prolate hemispheroid on a boundary with a hard medium

Figure 2.14b (right): The normalized modulus of a spectrum $|S_\Sigma(\nu)|$

We orient a hard prolate hemispheroid in such a way that its major semi-axis will be in the plane of an interface between the media. We calculate mirror-reflected pulses $\Psi_\Sigma(t')$, which occur at an angle of incidence $\theta_1 = 60°$, for two variants: 1) a hard prolate hemispheroid on a boundary with a hard medium and 2) a hard prolate hemispheroid on a boundary with a soft medium. Fig. 2-14a presents a pulse $\Psi_\Sigma(t)$ and a normalized modulus of a spectrum $|S_\Sigma(\nu)|$ for the first variant.

Fig. 2-15 shows the same characteristics for a second variant.

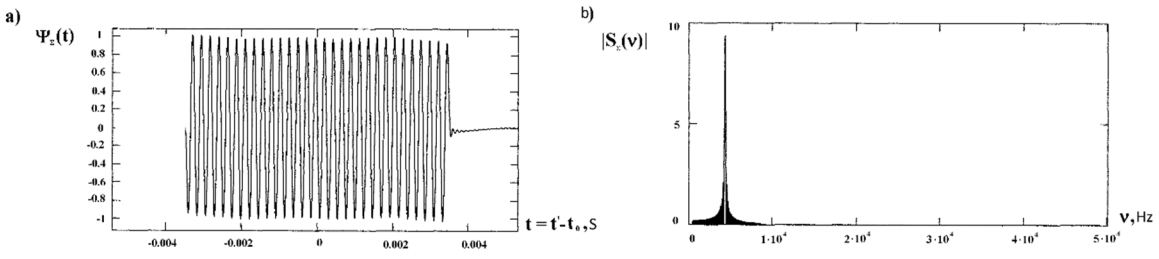

Figure 2-15a (left): A mirror reflection pulse $\Psi_\Sigma(t)$ for a hard prolate hemispheroid on a boundary with a soft medium

Figure 2.15b (right): The normalized modulus of a spectrum $|S_\Sigma(\nu)|$

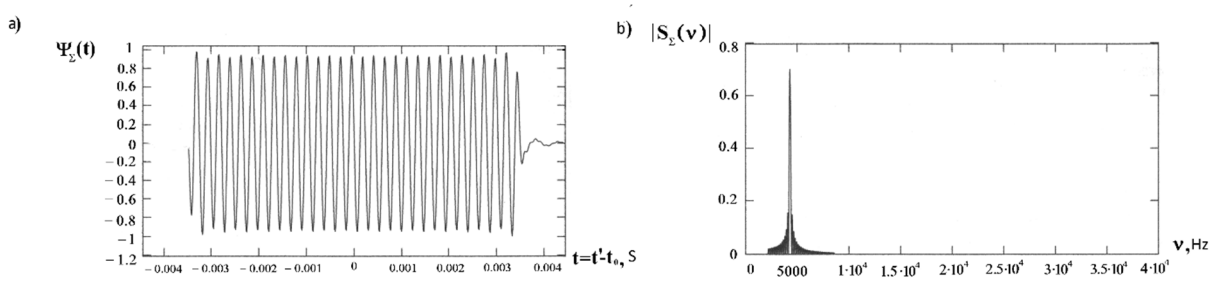

Figure 2-16a (left): A mirror reflection pulse$\Psi_\Sigma(t)$ for a hard oblate hemispheroid

Figure 2-16b (right): The normalized modulus of a spectrum $|S_\Sigma(\nu)|$ of a pulse $\Psi_\Sigma(t)$

We see in Fig. 2-16 a diffracted pulse $\Psi_\Sigma(t)$ and a modulus of its spectrum $|S_\Sigma(\nu)|$ in the direction of a mirror component for a hard oblate hemispheroid, which is located on the border between a liquid and an ideally soft medium in such a way that its major axis lies in a planar boundary. The angle of irradiation remains the same at$\theta_1 = 30°$.

Fig. 2-17 shows a diffracted pulse $\Psi_\Sigma(t)$ in the direction of a mirror component and a modulus of its spectrum $|S_\Sigma(\nu)|$ for a soft prolate hemispheroid placed on the border between a liquid and an ideally hard medium. The dimensions, the orientation of the hemispheroid, and the ratio of the semi-axis are the same as in Fig. 2-16. We note that for oblate and prolate hemispheroids located on an interface between the media, a diffracted pulse $\Psi_\Sigma(t)$ in the direction of a mirror component is obtained as a result of the interference between two reflected signals: the hemispheroid and the boundary. Therefore, it is designated as a diffracted pulse /.$\Psi_\Sigma(t)$.

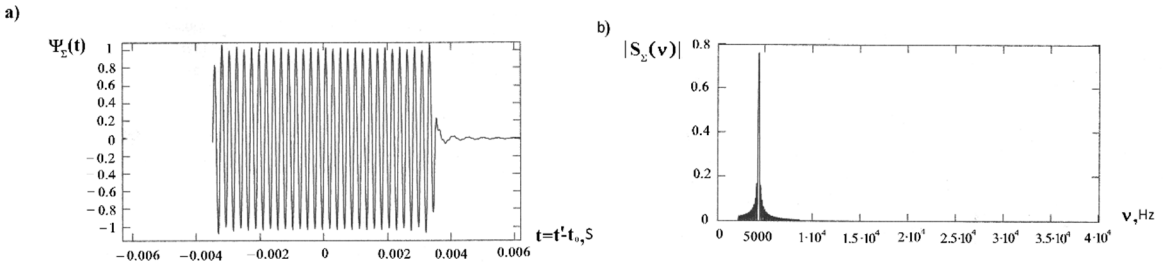

Figure 2-17a (left): The mirror reflection pulse$\Psi_\Sigma(t)$ for a soft prolate hemispheroid

Figure 2-17b (right): The normalized modulus of a spectrum $|S_\Sigma(\nu)|$ of a pulse $\Psi_\Sigma(t)$

Figure 2-17 depicts the sound's reflection by a spheroidal body located at the boundary between the liquid and an elastic bottom. We supplement these results with angular scattering characteristics $R(\theta, \phi)$ for a stationary sound signal with a fixed frequency.

2.2. An Ideal Spheroid in an Underwater Sound Channel

A study into the influence of two boundaries of the waveguide on the scattered field of a spheroidal scatterer will begin with an ideal spheroid placed in an underwater sound channel. The sound channel has non-reflective boundaries [32] and is irradiated with a pulsed signal with monochromatic filling [33]. At a depth z_0 of such a waveguide, we place a point source of an impulse signal and, at a horizontal distance r from that sound source, a spheroidal scatterer is placed at a depth of z_2 (Fig. 2-19a). A velocity profile of sound in a symmetrical underwater sound channel is shown in Fig. 2-19b. A receiver of a scattered signal is compatible with the sound source and so we will consider a combined system to find the spectrum of a scattered signal. Since, the velocity of sound depends only on vertical coordinate z, the rays in a horizontal plane are not bent. In each vertical half-plane, which passing through the center of a scatterer, a sound field will be independent of the adjacent half-planes and, at each half-plane, there will be complex coefficients from the excitation the modes of a sound channel. As a result, in each of these half-planes, one observes an interference pattern of modes independent of neighbouring half-planes. We are interested in a field in one vertical half-plane P, which contains the coincident point of a source-receiver and the center of a scatterer. Since a scattered field in this half-plane does not depend on the behavior of this field in all other half-planes, we shall take it to be the same in all vertical half-planes and equal to a field in half-plane P. The spectrum of a scattered signal at

the location of a source will be approximately (without taking into account the effect of the medium on an angular scattering characteristic) equal to [6]

$$S_2(\omega) = \rho_0^2(r_1)^{-1} \sum_{m=1}^{M} \sum_{n=1}^{N_m} P_m P_{n,m} D_{nm}(\omega)\, exp[-i(\kappa_m r_1 + \kappa_{nm} r_1 - \pi/2)] \text{ , (2.17)}$$

where $P_m = p_m(\rho_0)^{-1}\phi_m(z_2)\phi_m(z_0)$; p_m represents a mode excitation coefficient m; $\phi_m(z_2)$ represents an intrinsic waveguide function determined by boundary conditions; ρ_0 represents the density at the depth of the source and the receiver; $P_{nm} = (1/\rho_2)\phi_n(z_2)\phi_n(z_0)$; ρ_2- represents density at the depth of the centre of a scatterer; $D_{nm}(\omega)$ represents the space-transfer function of the scattering for an m-th mode of a source and an n-th mode of a scatterer; κ_m and κ_{nm} represent horizontal components of the wave numbers of modes of an incident and scattered waves, respectively; M represents the largest admissible source mode; and N represents the largest admissible scatterer mode for the m-th mode of a source.

The dependence of a sound velocity on a coordinate z for a symmetric waveguide (see Fig. 2-18 b) has the following form [32]:

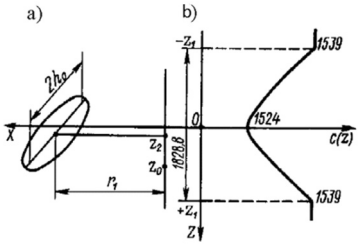

Figure 2-18 a (left): The mutual arrangement of a spheroidal scatterer and a source in a sound channel

Figure 2-18b Right): The profile of the velocity of sound in a sound channel with non-reflective boundaries

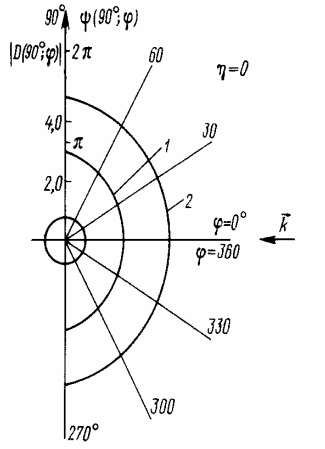

Figure 2-19: The amplitude-phase characteristic of sound scattering by a soft spheroid

We will find spectrum $S_2(\omega)$ located at the combined point of a source and the receiver for an ideal soft scatterer in the form of a prolate spheroid with a coordinate of an outer surface $\xi_0=1{,}005$. We place the combined system (source and receiver) on the axis of a symmetric waveguide ($z_2=z_0=0$), which is a major axis of the spheroid that is perpendicular to the Z-axis. An inter-focus spheroid distance (between the foci) $2h_0$ is assumed to be equal to 9,7 m. A source generates a pulse signal with a duration $\tau_0=0{,}05$ s at a frequency $f_0= 400$ Hz ($C=8{,}0$). The space-transfer function $D_{nm}(\omega)$ is determined by a picked frequency and, in an XOZ plane, the angular characteristics of a sound-scattering spheroid. With the chosen velocity profile of a sound (see Fig. 2-18b), one of the largest angles between wave vectors in the incident and scattered waves is approximately 16^o. Referring to the amplitude-phase angular characteristic of the scattering $D(\theta;\phi)$ from a sound wave reflected off a soft spheroid in an XOZ plane ($\theta = 90°,\ \eta = 0$) (see Fig. 2-19), we note that, even with a maximum wave size of ($C=10{,}0$), the angular characteristic $D(90°;\phi) = |D(90°;\phi)|\, exp[i\psi(90°;\phi)]$ is practically non-directional within angles $\phi = 0 \div 16°$ (see Fig. 2-19). Such an approach, in which modes of an underwater sound channel are considered in the form of plane waves

irradiating our spheroidal scatterer, is also approximate. Curve *1*, in Fig. 2-19, refers to $|D(90°;\phi)|$, while curve *2* characterizes a phase $\psi(90°;\phi)$ which is increased by π for all angles φ. At lower wave dimensions, its characteristics will be even closer to the circular form. Therefore, taking into account our assumption about a uniform scattering in a horizontal plane, we can assume that each incident wave from a set of admissible modes will uniformly scatter in all directions (as a non-directional scatterer) with an angular constant excitation coefficient $D(\omega)$, which then transfers the function $D_{nm}(\omega)$. As a result, the spectrum of a scattered signal will be calculated by means of the following formula [33]:

$$S_2(\omega) = D(\omega)\rho_0^2(r_1)^{-1}\sum_{m=1}^{M}\sum_{n=1}^{M} P_m P_{nm}\, exp[-i(\kappa_m r + \kappa_{nm} r - \pi/2)] \ . \quad (2.18)$$

2.3. The Diffraction of a Pulse Sound Signal on a Soft Prolate Spheroid Placed in a Planar Waveguide with a Hard Elastic Bottom

We turn to the familiar problem of the diffraction of pulses on spheroidal bodies in the planar waveguide [34–40]. These preserve the ideal soft upper boundary (the Dirichlet condition), waveguide dimensions, and scatterer with respect to the boundaries; they only replace the ideal hard lower boundary on the elastic isotropic bottom. Physical parameters of the lower medium will correspond to the isotropic elastic bottom but their values will be very close to the parameters of a transversely isotropic rock (a large slab of grey siltstone) [41]. The longitudinal wave velocity in this material is 4750 m/s, while the transverse wave velocity is 2811 m/s. Therefore, the method of imaginary sources needs the reflection of the coefficient V to be entered for each source [40] when displaying sources relative to the upper border sources. This [34–37, 41, 42] will change the sign of the source on the opposite side, which corresponds to a change of phase byπ.

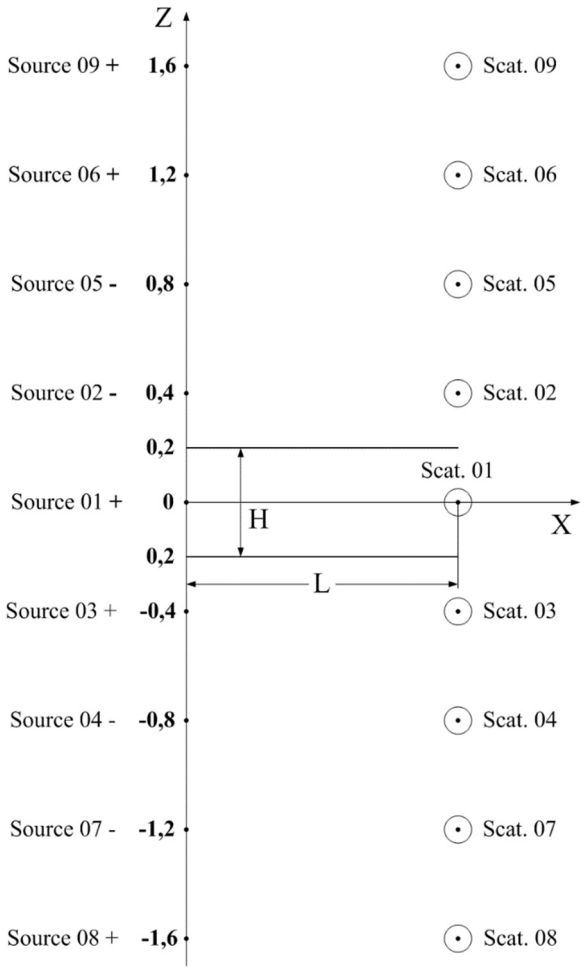

Figure 2-20: The mutual disposition of the pulse point sources and scatterers in the planar waveguide

It is known [40] that the imaginary sources method, used to calculate the boundary conditions, is not strictly fulfilled for any of the borders of the waveguide, even in the case of ideal Dirichlet and Neumann boundary conditions. For the better fulfillment of these conditions in diffraction problems [7, 34–37, 41, 42], imaginary

scatterers were introduced by mirroring their relative waveguide boundaries. Likewise, we introduce imaginary scatterers to compare with the reflection of such pulses [7, 34, 35] in the ideal borders and in the presence of a hard elastic bottom in the waveguide. [40] shows that the method of imaginary sources is applicable in the case where the reflection coefficient V will be a function of the angle in the wave, which is from a source relative to the normal (perpendicular) boundary. In our case, this angle will be determined by the mutual position of the source (whether real or imaginary) and the scatterers (real or imaginary), where the wave falls from the source. Since the receiver is combined with a real source Q, the sequence of the reflected pulses will be determined by the quantity and the amplitudes of the reflected signals (from different scatterers), which have the same propagation time as the waves that travel from sources to scatterers and from scatterers to point Q. The parameters of the waveguide, the position of the real source Q (combined with the receiver), and the position of the real scatterer remain unchanged as in [7, 34, 35]: L = 1000 m. and H = 400 m. The real source Q and the real scatterer are each located at a depth of 200 m. The scatterer is an ideal soft prolate spheroid with a semi-axes ratio of a/b = 10 (a = 0,279 m.). Its axis of rotation is perpendicular to the plane of the figure (see Fig. 2-20). The formula for the reflection coefficient V_{0N}, where N represents the number of a source, is given in [40]. For the calculation of the first four reflected pulses, the following reflection coefficients are needed: V_{03}, in the direction of the first (real) scatterer 01; V_{05}, in the direction of the second (imaginary) scatterer 02. As a result of simple calculations made with the help of [10], we obtain: V_{03}= 0,8423 + i 0,5390; V_{05}=0,8423 + i 0,5390.

Coefficients have become complex. This means that the total internal reflection is at the boundary between the liquid and the hard elastic bottom. Therefore, modules of reflection coefficients are equal to 1,0 and the real parts of the coefficients are close to +1,0, which is typical for the boundary between a liquid and an absolutely hard bottom. The resulting sequence of calculations of first four reflected pulses is shown in Fig. 2-21.

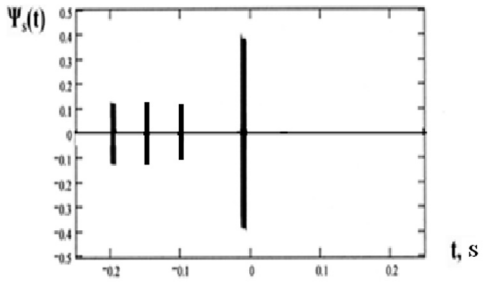

Figure 2-21: The normalized series of first four reflected impulses in a waveguide with a hard elastic bottom

We compared this sequence to the sequence in Fig. 2-22, where there are ideal boundaries [7, 34, 35]:

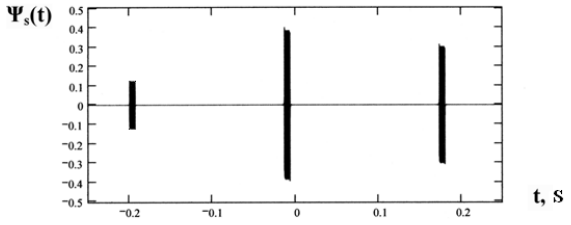

Figure 2-22: The normalized series of the first three reflected impulses with harmonic filling in point Q

The first and fourth pulses of Fig. 2-21 are identical to the first and second pulses of Fig. 2-22. As for the second and third pulses shown in Fig. 2-21, in the case of ideal boundaries and the symmetrical location of a real source and a real scatterer relative to the boundaries of the waveguide, they are compensated (absorb each other) by each of the reflected pulses: i. e., the second and third, pulses (see Fig. 2-21). This shows the difference in the sequences of the reflected pulses when replacing an absolutely hard bottom with that of an elastic hard bottom. Exactly the same result is obtained for the anisotropic (transversely isotropic) bottom, if its isotropy plane coincides with the plane of the impulse incidence.

A similar pattern is observed for an anisotropic bottom, such as one composed of silicon, where there is a quasi-longitudinal wave velocity of about 8300 m/s and a quasi-transverse wave velocity of about 5700 m/s [39]. Due to the high velocities of the quasi-longitudinal and quasi-transverse waves, the total internal reflection effect at the anisotropic bottom manifests itself even more strongly than at the isotropic bottom.

2.4. The Diffraction of a Pulse Sound Signal on a Non-Analytical Elastic Scatterer Put in Planar Waveguide with a Hard Elastic Bottom

Based on the obtained solution, let us consider the more general problem of the pulsed sound signal diffraction that impacts on an elastic scatterer comprised of a finite cylindrical shell supplemented with two hemispherical shells (one on either end) (Fig. 2-23) and placed in a waveguide with a hard elastic bottom (Fig. 2-24). Here, the data was calculated using integral equations [7, 43–47]. We note that a similar problem can be solved with the help of other methods: the boundary element method [46, 48]; the T-matrix method [49]; the method of a potential [50]; the finite element method [51]; and the Green's function method [52].

The first stage will solve the problem of the diffraction of a harmonic wave on such a shell.

The density of the material of the shell is ρ_1 and the Lame's coefficients are λ and μ. The shell was internally filled with the internal liquid medium with a density of ρ_2 and a sound velocity of C_3. It was placed in an external liquid medium with a density of ρ_0 and a sound velocity of C_0. As the shell falls, the plane harmonic wave has the pressure p_i under the angle Θ_0 and with the wave vector $\vec{k}$.

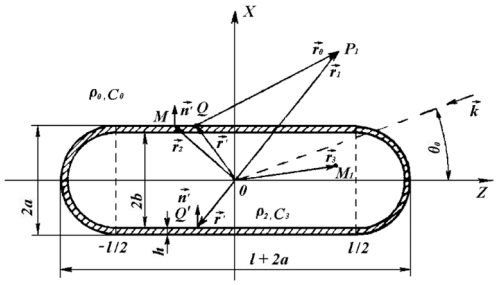

Figure 2-23: The elastic shell in the form of a terminal cylinder ending with semi-spheres

As was shown in [7] and [43–47], the initial equation is an integral equation having the sense of the generalized Huygen's principle for the displacement vector $\vec{u}(\vec{r})$ of the elastic shell:

$$\vec{u}(\vec{r}) = \iint_S \left\{ \vec{t}(\vec{r}')G(\vec{r}';\vec{r}) - \vec{u}(\vec{r}')\left[\hat{n}'\sum(\vec{r}';\vec{r})\right]\right\} dS(\vec{r}'), \quad \vec{r} \in V, \qquad (2.19)$$

where $\vec{t}(\vec{r}') = \hat{n}'T(\vec{r}')$ is the stress vector; $\hat{n}' \equiv \hat{n}'(\vec{r}') = \vec{n}'(\vec{r}')$ is the single vector of the external along the relation to S normal; $T(\vec{r}')$ is the stress tensor of the isotropic material; $G(\vec{r}';\vec{r})$ is the Green's displacement tensor; and $\sum(\vec{r}';\vec{r})$ is the Green's stress tensor. Additionally, if $\vec{r}$ is the point of surface S, then the left part of equation (2.19) will be $\vec{u}(\vec{r}')/2$.

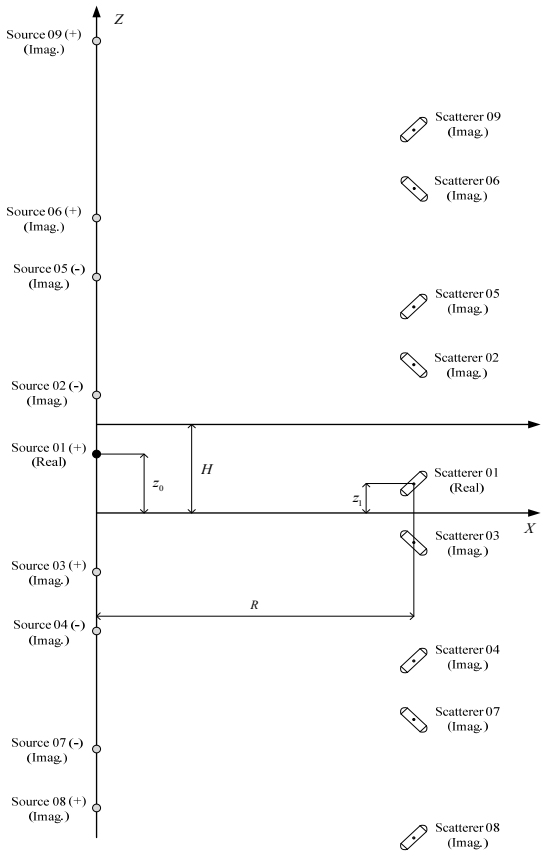

Figure 2-24: The mutual disposition of the impulse point sources and scatterers in the planar waveguide

The displacement vector $\vec{u}(\vec{r})$, the stress tensor$T(\vec{r})$, the Green's displacement tensor $G(\vec{r}';\vec{r})$, and the Green's stress tensor $\Sigma(\vec{r}';\vec{r})$ were connected by the following correlations [7, 47]:

$$T(\vec{r}) = \lambda I \nabla \vec{u}(\vec{r}) + \mu(\nabla \vec{u} + \vec{u}\nabla) \ , \qquad (2.20)$$

$I = I_L + I_T$; $I_L = (\nabla\nabla)/\nabla^2$; $I_L \cdot I_T = 0$; and $I_T = -[\nabla(\nabla I)]/\nabla^2$, where I_L and I_T are the longitudinal and transverse single tensors for the Hamilton's operator ∇:

$$\sum(\vec{r}';\vec{r}) = \lambda I \nabla G(\vec{r}';\vec{r}) + \mu\left[\nabla G(\vec{r}';\vec{r}) + G(\vec{r}';\vec{r})\nabla\right] \ ; \qquad (2.21)$$

$$G(\vec{r}';\vec{r}) = (1/4\pi\rho_t\omega^2)\{k_2 I g(k_2|\vec{r}' - \vec{r}|) + \\ +\nabla'[g(k_1|\vec{r}' - \vec{r}|) - g(k_2|\vec{r}' - \vec{r}|)]\nabla\} \ , \qquad (2.22)$$

where k_1 and k_2 are the wave numbers of the longitudinal and transverse waves in the material of the shell.

The second integral equation presents the Kirchhoff integral for the diffracted pressure $p_\Sigma(P_1)$ in the external medium:

$$C(P_1)p_\Sigma(P_1) = -\iint_{S_a}\{p_\Sigma(Q)(\partial/\partial n')[exp(ikr_0/r_0)] - \\ -[exp(ikr_0/r_0)]\rho_0\omega^2(\vec{u}\vec{n}')\}dS_a + 4\pi p_i(P_1) \ , \qquad (2.23)$$

where $p_\Sigma(P_1) = p_i(P_1) + p_s(P_1)$; $p_s(P_1)$ is the scattered pressure at point P_1; $C(P_1)$ is the numerical coefficient, equal to 2π if $P_1 \in S_a$ or 4π, if P_1 is outside of S_a; S_a is the external surface of the shell; and Q is the point located on the external surface of the shell.

For the pressure $p_2(M_1)$ in the internal liquid medium at point M_1, the third integral equation is derived:

$$C(M_1)p_2(M_1) = \iint_{S_b}\{p_2(Q')(\partial/\partial n')[exp\,(ikr_3)/r_3] -$$